conductivity due to thermal motions of the lattice, the hole contribution will dominate. As the temperature is lowered below 160 K, deexcitation of electrons from bands 2 and 3 to band 1 will remove the holes of band 1. Further, thermal motions of the lattice are reduced. Thus, electrons of band 2 contribute significantly to conductivity, so that the $CsP_8W_8O_{40}$ bronze is metallic and its carriers are electrons below 160 K. The resistivity upturn at ~24 K can be ascribed to a charge density wave (CDW) associated with the one-fourth filled band 2, since it is a strongly one-dimensional one. It should be possible to observe a CDW with vector $q_{CDW} \approx 0.25c^*$.

**B. $Cs_{1-x}P_8W_8O_{40}$.** Figure 2 shows that the resistivity hump of $Cs_{1-x}P_8W_8O_{40}$ (at ~160 K for $x = 0$) is gradually shifted to a lower temperature as $x$ increases toward 0.5 and that, at $x \approx 0.5$, the bronze becomes semiconducting at all temperatures. These observations can be explained as follows: as $x$ increases from 0.0 to 0.5, the number of electrons in band 2 decreases from 0.5 to 0.25. As the electron density in band 2 decreases, screening among the electrons of the band is reduced, so that the electrons become more susceptible toward localization around $Cs^+$-rich neighbors. Therefore, even electrons of band 2 may require activated conductivity. Thus, the resistivity hump of $Cs_{1-x}P_8W_8O_{40}$ is gradually shifted to a lower temperature as the Cs content is decreased, and beyond a certain value of $x$, the bronze becomes semiconducting.

**C. $Cs_xA_yP_8W_8O_{40}$ (A = Rb, Na).** Figure 4 shows that, in contrast to $Cs_{1-x}P_8W_8O_{40}$, the $Cs_xA_yP_8W_8O_{40}$ bronze does not have a resistivity hump when measured along the $c$ crystallographic direction. For the partially substituted bronze, $x + y > 1$, so that it has more d electrons than does $CsP_8W_8O_{40}$. In diagram **3**, which is applicable for $x + y = 1$, thermal excitation probability is large for the excitation to the bottom of band 3, as already mentioned. Thus, provided that the $x + y$ value of the Rb- and Na-substituted bronze is large enough to fill the bottom portion of band 3, thermal excitation from band 1 would be weak. Then the hole contribution to conductivity from band 1 is diminished so that electron contribution from band 2 becomes dominant. As a result, the resistivity hump along the $c$ axis found for $Cs_{1-x}P_8W_8O_{40}$ will be absent in $Cs_xA_yP_8W_8O_{40}$ ($x + y > 1$). The sample-dependent semiconductor-to-metal transition seen in the resistivity of $Cs_xA_yP_8W_8O_{40}$ samples in the *ab* plane cannot be accounted for in terms of the band diagram, and its origin is not clear.

**D. $CsP_8W_{8-x}Mo_xO_{40}$.** According to Figure 5, the metallic character of $CsP_8W_8O_{40}$ quickly disappears when a small amount of W is substituted with Mo. This result is expected since the random distribution of Mo atoms in the $W_4O_{18}$ chains will disrupt the band electron contribution to conductivity.

## Concluding Remarks

$CsP_8W_8O_{40}$ exhibits a broad resistivity hump at ~160 K and a resistivity upturn at ~24 K. To examine the origin of these resistivity anomalies, we prepared its electron-deficient and electron-rich analogues ($Cs_{1-x}P_8W_8O_{40}$ and $Cs_xA_yP_8W_8O_{40}$ ($x + y > 1$), respectively), measured their physical properties, and performed tight-binding band electronic structure calculations on the $P_8W_8O_{40}^-$ lattice. The present work suggests the ~160 K resistivity hump to be due to the fact that the Fermi level of the $P_8W_8O_{40}^-$ lattice, which occurs near the bottom of dispersive one-dimensional bands, lies very close to the top of flat, filled bands and also very close to the bottom of dispersive, one-dimensional, empty bands. Our study also suggests that the resistivity upturn of Cs at ~24 K stems from a CDW associated with the dispersive one-dimensional bands.

**Acknowledgment.** We thank Dr. J. S. Delaney for the electron microprobe analysis of Cs in the samples. Work at Rutgers University was supported by the National Science Foundation-Solid State Chemistry Grants DMR-84-04003 and DMR-87-14072 and the National Science Foundation Materials Research Instrumentation Grants DMR-84-08266 and DMR-87-05620. Work at the Universite de Paris-Sud and North Carolina State University was supported by NATO, Scientific Affairs Division, and also by DOE, Office of Basic Sciences, Division of Materials Science, under Grant DE-FG05-86ER45259.

---

Contribution from the Laboratoire de Chimie Theorique, Universite de Paris-Sud, 91405 Orsay, France, and Departments of Chemistry, Rutgers, The State University of New Jersey, New Brunswick, New Jersey 08903, and North Carolina State University, Raleigh, North Carolina 27695-8204

# Structural and Electronic Origin of the Three-Dimensional Electrical Properties of $P_8W_{12}O_{52}$ and Its Inserted and Substituted Analogues $A_xP_8W_{12}O_{52}$ (A = Li, Na) and $P_8W_{12-x}Mo_xO_{52}$

Enric Canadell,*[†] Idris El-Idrissi Rachidi,[†] Enoch Wang,[‡] Martha Greenblatt,*[‡] and Myung-Hwan Whangbo*[§]

*Received November 21, 1988*

Single crystals of $P_8W_{12}O_{52}$ and its inserted and substituted analogues $A_xP_8W_{12}O_{52}$ (A = Li, $x = 0.16$; A = Na, $x = 0.22$) and $P_8W_{12-x}Mo_xO_{52}$ ($x = 0.28$, 0.40, 0.68) were prepared, and their electrical resistivities and magnetic susceptibilities were measured. All of these bronzes are found to be isotropic metals. Our tight-binding band electronic structure calculations on $P_8W_{12}O_{52}$ show that the three-dimensional metallic character originates from a three-dimensional linking of $WO_6$ octahedra in the lattice and the relatively high oxidation state of W. Examination of the structural relationship between $P_8W_{12}O_{52}$ and $CsP_8W_8O_{40}$ led to a new synthetic route for the preparation of $CsP_8W_8O_{40}$ from $P_8W_{12}O_{52}$. With use of this new method, $Tl_2P_8W_8O_{40}$ (isostructural with $CsP_8W_8O_{40}$) was synthesized for the first time.

## Introduction

Tungsten bronzes of the diphosphate ions $P_2O_7^{4-}$ have open framework channel structures, in which alkali-metal and other metal ions can be intercalated. So far, three types of channel structures have been identified in diphosphate tungsten bronzes: $CsP_8W_8O_{40}$ has octagonal channels,[1] a family of $A_x(P_2O_4)_4(WO_3)_{4m}$ (A = K with $m = 5$–11;[2] A = Rb with $m = 4$–11;[3] A = Tl with $m = 8$;[4] A = Ba with $m = 6$–10[5]) has hexagonal

[†] Universite de Paris-Sud.
[‡] Rutgers University.
[§] North Carolina State University.

(1) Goreaud, M.; Labbe, Ph.; Raveau, B. *J. Solid State Chem.* **1985**, *56*, 41.
(2) Hervieu, M.; Raveau, B. *J. Solid State Chem.* **1982**, *43*, 291.
(3) Giroult, J. P.; Goreaud, M.; Labbe, Ph.; Raveau, B. *Acta Crystallogr.* **1982**, *B38*, 2342.

0020-1669/89/1328-2455$01.50/0 

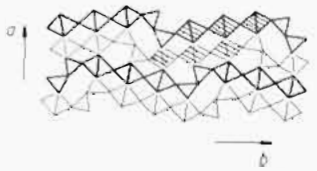


**Figure 1.** Projection view of $P_8W_{12}O_{52}$.

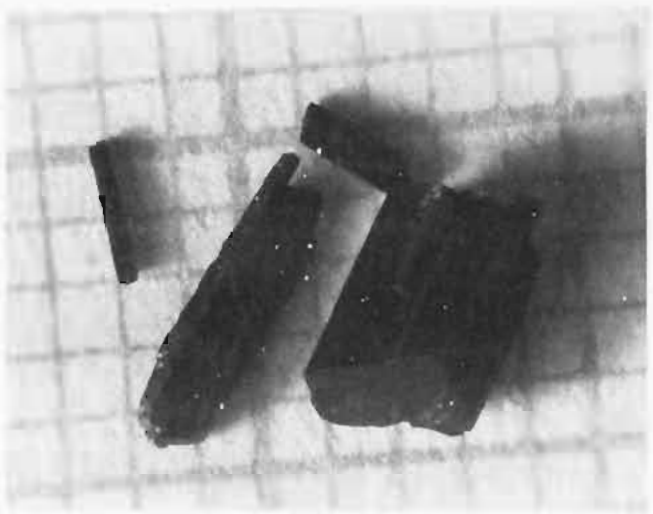

**Figure 2.** $P_8W_{12}O_{52}$ crystals (small squares are 1 × 1 mm²).

channels, and $P_8W_{12}O_{52}$[6] has both pentagonal and hexagonal channels. In the present work, we prepared $P_8W_{12}O_{52}$ and its substituted analogues $A_xP_8W_{12}O_{52}$ (A = Li, Na) and $P_8W_{12-x}Mo_xO_{52}$ and found a synthetic route to the new bronzes $A_xP_8W_8O_{40}$ (A = Rb, Tl, Cs) from $P_8W_{12}O_{52}$. Measurements of the electrical resistivities and magnetic susceptibilities of $P_8W_{12}O_{52}$ and its substituted analogues reveal that they are not low-dimensional metals, in contrast to the case for all other known monophosphate and diphosphate tungsten bronzes. We account for this observation by performing tight-binding band electronic structure calculations on the $W_4O_{18}$ chain (**3**), the $W_6O_{28}$ chain (**2**), and the $W_{12}O_{48}$ lattice (Figure 1) present in $P_8W_{12}O_{52}$.

## Experimental Section

A stoichiometric mixture of $(NH_4)_2HPO_4$ and $WO_3$ needed for $P_8W_{12}O_{52}$ was first heated in air at ~650 °C to decompose the phosphate. Then an appropriate amount of W metal was added to the initially decomposed product (i.e., the molar stoichiometric mixture initially reacted was $P_2O_5$:$WO_3$ = 4:(32/3) and another $^4/_3$ W was added to obtain the final product). The final mixture was then pelletized and heated to 1100 °C in an evacuated quartz tube for about 4 days and then slowly cooled to room temperature in 4 days.[6] This technique, as reported by Domenges et al.,[5] leads to polycrystalline $P_8W_{12}O_{52}$ only. However, large single crystals of $P_8W_{12}O_{52}$ can be obtained from the synthesis of $CsP_8W_8O_{40}$. We found that large, red, single crystals of $P_8W_{12}O_{52}$ are grown along with the $CsP_8W_8O_{40}$ crystals in the $CsP_8W_8O_{40}$ synthesis. Similarly, polycrystalline and single-crystal samples of partially Mo-substituted $P_8W_{12-x}Mo_xO_{52}$ and alkali-metal-inserted $A_xP_8W_{12}O_{52}$ (A = Li, Na) were obtained from the $CsP_8W_{8-x}Mo_xO_{40}$ and $Cs_{0.8}A_{0.2}P_8W_8O_{40}$ (A = Li, Na, Rb) synthesis. All phases were identified by powder X-ray diffraction with a Scintag PAD V system with monochromatized Cu K$\alpha$ radiation and Si as an internal standard.

Standard, four-probe, low-temperature (2–270 K) dc resistivity measurements were made on oriented single crystals of $P_8W_{12}O_{52}$. Electrical contacts were made with ultrasonically evaporated indium. Magnetic susceptibilities of single crystals were measured on a Quantum Design SQUID magnetometer between 4 and 260 K. Elemental analysis was performed with a Beckman plasma emission spectrometer.

Tight-binding band electronic structure calculations[7] were performed on the $W_{12}O_{48}$ lattice within the framework of the extended Hückel method.[8] The atomic parameters employed in the present work were taken from our previous work.[9,10]

## Crystal Structure

The crystal structure of $P_8W_{12}O_{52}$ can be conveniently described in terms of the $W_3O_{16}$ cluster shown in **1**, which is made up of three $WO_6$ octahedra by sharing axial oxygen atoms. Such

**1**

clusters lead to the $W_6O_{28}$ chain **2a** by sharing their equatorial

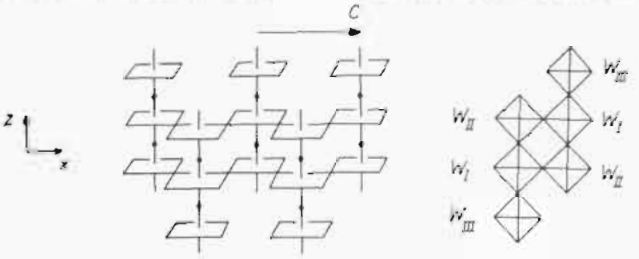


**2a** **2b**

oxygen atoms. A projection view of **2a** along the chain axis is given by **2b**. As shown in Figure 1, the three-dimensional (3D) structure of $P_8W_{12}O_{52}$ is obtained by the $W_6O_{28}$ chains and $P_2O_7^{4-}$ anions (indicated by triangles in Figure 1) upon sharing their oxygen atoms. From **2** and Figure 1, one finds three types of tungsten atoms, $W_I$, $W_{II}$, and $W_{III}$. It is noted that the $W_IO_6$ and $W_{II}O_6$ octahedra form the double-zigzag chain $W_4O_{18}$ (**3**), which

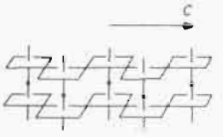


**3**

is represented by the middle four $WO_6$ octahedra of every $W_6O_{28}$ chain shown by shading in Figure 1. It is the $W_{III}O_6$ octahedra that link the $W_4O_{18}$ chains together to form the 3D lattice $W_{12}O_{48}$, i.e., $P_8W_{12}O_{52}$ without the diphosphate units. In each $WO_6$ octahedron, $W_I$, $W_{II}$, and $W_{III}$ respectively share two, one, and three oxygen atoms with the diphosphate anions and the remaining oxygen atoms with other $WO_6$ octahedra.

According to a Zachariasen-type analysis of the W–O bond lengths of $WO_6$ octahedra,[11] the oxidation states of $W_I$, $W_{II}$, and $W_{III}$ are calculated to be 5.19, 5.10, and 5.71, respectively. Thus,

(4) Giroult, J. P.; Goreaud, M.; Labbe, Ph.; Raveau, B. *Mater. Res. Bull.* **1981**, *16*, 811.
(5) Lamire, M.; Labbe, Ph.; Goreaud, M.; Raveau, B. *J. Solid State Chem.* **1987**, *71*, 342.
(6) Domenges, B.; Gareaud, M.; Labbe, Ph.; Raveau, B. *Acta Crystallogr.* **1982**, *B38*, 1724.
(7) Whangbo, M.-H.; Hoffmann, R. *J. Am. Chem. Soc.* **1978**, *100*, 6093.
(8) Hoffmann, R. *J. Chem. Phys.* **1963**, *39*, 1397. A modified Wolfsberg–Helmholz formula was used to calculate the off-diagonal $H_{ij}$ values. See: Ammeter, J. H.; Burgi, H.-B.; Thibeault, J.; Hoffmann, R. *J. Am. Chem. Soc.* **1978**, *100*, 2686.
(9) Wang, E.; Greenblatt, M.; El-Idrissi Rachidi, I.; Canadell, E.; Whangbo, M.-H. *Inorg. Chem.*, preceding paper in this issue.
(10) Wang, E.; Greenblatt, M.; El-Idrissi Rachidi, I.; Canadell, E.; Whangbo, M.-H. *J. Solid State Chem.*, in press.
(11) Domenges, B.; McGuire, N. K.; O'Keeffe, M. *J. Solid State Chem.* **1985**, *56*, 94.

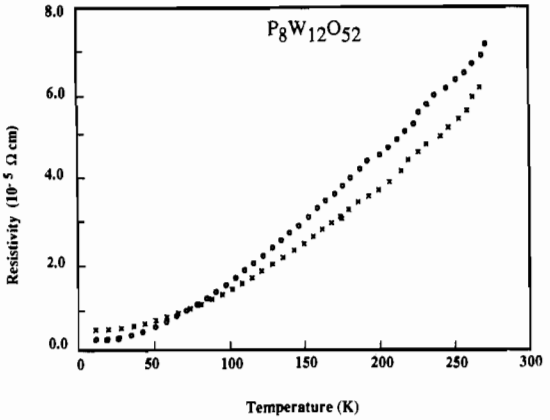


**Figure 3.** Temperature-dependent resistivity of a $P_8W_{12}O_{52}$ crystal along the length (○) and sides (×).

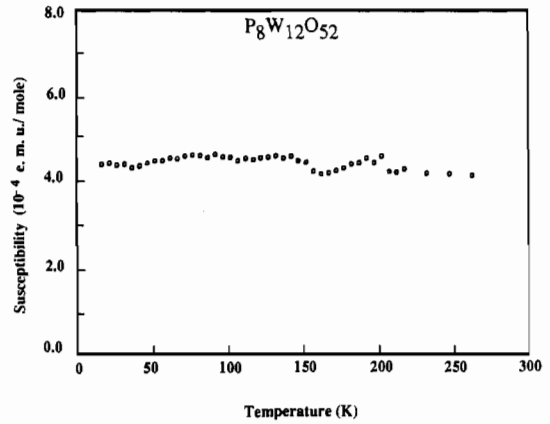


**Figure 4.** Magnetic susceptibility of a $P_8W_{12}O_{52}$ crystal. The applied magnetic field ($H$) was 1 T.

one might expect a negligible contribution of $W_{III}$ in the low-lying d-block bands of $P_8W_{12}O_{52}$ and hence a low-dimensional electrical property. However, this is contrary to our experimental results, as will be discussed later. With the formal oxidation states of $O^{2-}$ and $P_2O_7^{4-}$, one finds eight d electrons per 12 W atoms, i.e., four electrons per $W_6O_{28}$ chain (**2**). Tungsten in $P_8W_{12}O_{52}$ has a relatively high average oxidation state (i.e., +5.33).

## Results and Discussion

**Synthesis and Physical Properties. A. $P_8W_{12}O_{52}$.** Red chunky crystals of $P_8W_{12}O_{52}$ (Figure 2) with an average size of 4.7 × 0.8 × 0.9 mm$^3$ were obtained from the $CsP_8W_8O_{40}$ synthesis. The majority of the red $P_8W_{12}O_{52}$ crystals formed in the hot zone, while the golden crystals of $CsP_8W_8O_{40}$ were found only in the cold zone of the quartz tube. The length of the chunky crystals employed in the resistivity measurements was found to correspond to the short, $c$ crystallographic axis while the sides corresponding to the $a$ and $b$ axes were not well-defined by the morphology of the crystals. However, repeated resistivity measurements reveal no anisotropy between the length and the sides of the crystal. Room-temperature resistivities are $\rho_{length} = 7.3 \times 10^{-5}$ Ω cm and $\rho_{sides} = 6.5 \times 10^{-5}$ Ω cm. Hence, $P_8W_{12}O_{52}$ is indeed an isotropic electronic conductor. The temperature-dependent resistivity shown in Figure 3 indicates a metallic behavior and no anomaly in the temperature range studied (2–300 K). Similarly, metallic behavior was confirmed by the Pauli paramagnetism of the magnetic susceptibility measurement (see Figure 4). In addition, $P_8W_{12}O_{52}$ is highly conductive, with a conductance of $\sim 1.5 \times 10^4$ Ω$^{-1}$ cm$^{-1}$. It is the most conductive phosphate tungsten bronze known.

**B. $P_8W_{12-x}Mo_xO_{52}$.** Single crystals or polycrystalline samples of partially Mo-substituted $P_8W_{12-x}Mo_xO_{52}$ ($x$ = 0.28, 0.40, 0.68) bronzes were obtained along with the $CsP_8W_{8-x}Mo_xO_{40}$ bronze crystals (see Experimental Section). In $P_8W_{12-x}Mo_xO_{52}$ bronzes, as the Mo contents increased the unit cell volume decreased (Table I). A similar trend was observed in the $CsP_8W_{8-x}Mo_xO_{40}$ bronzes.

**Table I.** Cell Parameters of $P_8W_{12-x}Mo_xO_{52}$

| compd | $a$, Å | $b$, Å | $c$, Å | $V$, Å$^3$ |
|---|---|---|---|---|
| $P_8W_{12}O_{52}$ | 11.99 (2) | 15.58 (1) | 5.327 (7) | 995.3 (0.8) |
| $P_8W_{11.72}Mo_{0.28}O_{52}$ | 11.97 (1) | 15.60 (2) | 5.313 (2) | 992.5 (1.2) |
| $P_8W_{11.60}Mo_{0.40}O_{52}$ | 11.98 (1) | 15.56 (1) | 5.319 (4) | 991.2 (0.9) |
| $P_8W_{11.32}Mo_{0.68}O_{52}$ | 11.96 (2) | 15.57 (1) | 5.315 (8) | 989.3 (1.0) |

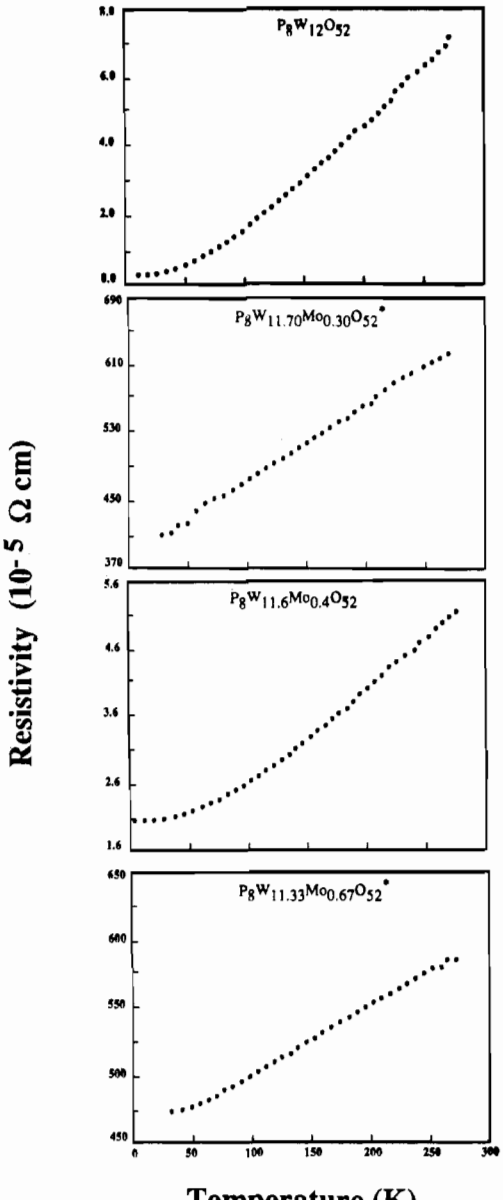


**Figure 5.** Temperature-dependent resistivity of $P_8W_{12-x}Mo_xO_{52}$ bronzes (asterisks denote a polycrystalline sample).

However, the electronic properties of $P_8W_{12-x}Mo_xO_{52}$ do not differ from those of the host, $P_8W_{12}O_{52}$. In $P_8W_{12-x}Mo_xO_{52}$ bronzes, the temperature-dependent resistivity indicates a metallic behavior with no anomaly up to $x$ = 0.68 (Figure 5). In other low-dimensional phosphate tungsten bronzes, either a metal–semiconductor transition (e.g. $KP_8W_{24-x}Mo_xO_{88}$) or only semiconducting behavior (e.g. $CsP_8W_{8-x}Mo_xO_{40}$ and $P_4W_{12-x}Mo_xO_{44}$) is observed at such a large Mo:W ratio. Attempts so far to synthesize $P_8W_{12-x}Mo_xO_{52}$ with a Mo concentration higher than $x$ = 0.68 have been unsuccessful. Therefore, the critical Mo contents (if any) could not be determined.

**C. $A_xP_8W_{12}O_{52}$ (A = Li, Na).** Alkali-metal-inserted $Li_{0.16}P_8W_{12}O_{52}$ and $Na_{0.22}P_8W_{12}O_{52}$ red bronzes were obtained along with the partially substituted $Cs_xA_yP_8W_8O_{40}$ (A = Na, Rb; $x + y \approx 1$) golden bronzes during a synthesis of compositions intended to be $Cs_{0.8}A_{0.2}P_8W_8O_{40}$ (A = Li, Na, Rb) bronzes. Interestingly,

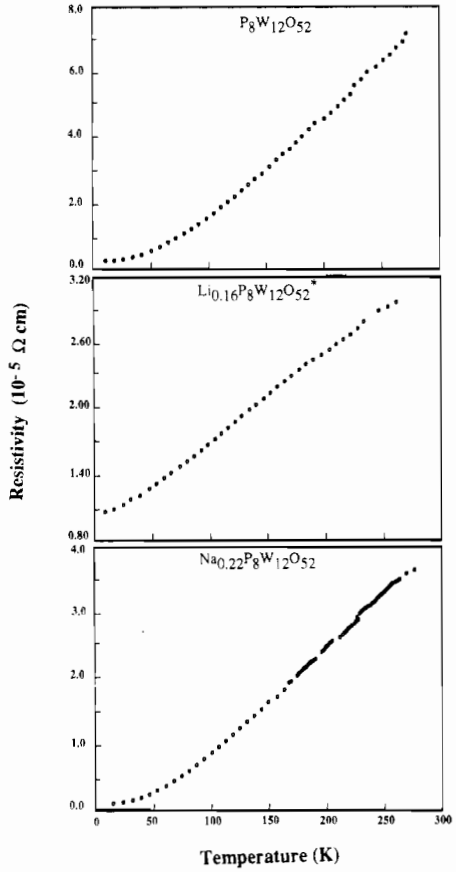


**Figure 6.** Temperature-dependent resistivity of $A_xP_8W_{12}O_{52}$ (A = Li, Na; the asterisk denotes a polycrystalline sample).

the distribution of the inserted cations between the red and golden phases is dependent on the sizes of the cations to be inserted and the sizes of the different tunnels between the two types of bronzes. A small ion such as $Li^+$ is found almost exclusively (>98%) in the red $P_8W_{12}O_{52}$ phase; a large ion such as $Rb^+$ is found almost exclusively (>98%) in the $CsP_8W_8O_{40}$ phase as determined by chemical analysis; a medium-sized ion such as $Na^+$ is distributed evenly between the two phases. $Rb^+$ ions are clearly too large for the small cavities found in $P_8W_{12}O_{52}$ while $Li^+$ is too small and too polarizing and tends to destabilize the $CsP_8W_8O_{40}$ structure as previously discussed.[12]

The electronic properties of the alkali-metal-inserted $A_xP_8W_{12}O_{52}$ are similar to those of the host, $P_8W_{12}O_{52}$. A metallic behavior with conductivity similar to that of the host was observed (Figure 6). No anisotropy was detected in the single crystals of $Na_{0.22}P_8W_{12}O_{52}$ (an orientation study on the electronic properties of $Li_{0.16}P_8W_{12}O_{52}$ was not possible since large single crystals of $Li_{0.16}P_8W_{12}O_{52}$ were not obtained). In an attempt to synthesize Na-rich $Na_xP_8W_{12}O_{52}$, an interesting intergrowth was observed in the composition intended to be $Na_2P_8W_{12}O_{52}$: Huge crystals ($4 \times 1.5 \times 0.8$ mm$^3$) of $Na_xP_4W_8O_{32}$ ($x = 1.3, 1.5$), a $MPTB_h$ (i.e., a monophosphate tungsten bronze with hexagonal tunnels, which is made up of $ReO_3$-type $WO_6$ corner-sharing octahedral slabs connected by $PO_4$ tetrahedra, creating large hexagonal tunnels in the 3D network) phase,[13] were found to be the predominant phase, and $Na_xP_8W_{12}O_{52}$ was determined to be the minor phase. This provides a new synthetic route for obtaining large single crystals of $MPTB_h$ for the characterization of electronic properties. Reasons for the intergrowth are still unknown at present but are likely due to similarities of the structures of the phases involved.

**D. $A_xP_8W_8O_{40}$ (A = Rb, Tl, Cs).** During our investigation of the structural properties of $P_8W_{12}O_{52}$, a new synthetic route was discovered for the synthesis of new $A_xP_8W_8O_{40}$ (A = Rb, Tl, Cs) bronzes with octagonal tunnels from the $P_8W_{12}O_{52}$ bronze. The $CsP_8W_8O_{40}$ and $P_8W_{12}O_{52}$ bronzes are closely related structurally, as evidenced by the intergrowth of $P_8W_{12}O_{52}$ and $CsP_8W_8O_{40}$; we decided to undertake a study of the phase transformations between these two structural types according to the reaction

$$P_8W_{12}O_{52} + CsI \xrightarrow{5\%\ KBr} CsP_8W_8O_{40} + \tfrac{1}{2}I_2 + 4WO_3$$

A mixture of polycrystalline $P_8W_{12}O_{52}$, CsI, and 5% KBr was pelletized and sealed (under vacuum) in a quartz tube. The mixture was slowly heated to 850 °C for ~3 days before slow annealing to room temperature over about 6 days. After the reaction some iodine vapor was observed. In addition, golden crystals were deposited on the cold end of the tube, while some red $P_8W_{12}O_{52}$ and a white amorphous phase (possibly $WO_3$) remained in the hot end. The golden phase was identified by powder X-ray diffraction to be isostructural with $CsP_8W_8O_{40}$, with the composition $Cs_{0.67}P_8W_8O_{40}$. This interesting result prompted us to investigate the possibility of substituting for Cs other large cations such as $Rb^+$ and $Tl^+$. Indeed, not only were we able to synthesize the previously reported $Rb_xP_8W_8O_{40}$[14] bronze but we also obtained $Tl_2P_8W_8O_{40}$ (isostructural with $CsP_8W_8O_{40}$) for the first time using TlCl. Work is in progress to obtain large single crystals of $Tl_2P_8W_8O_{40}$ for characterization of their electronic properties. Thus, this new synthetic method affords a versatile and low-temperature route for the synthesis of the interesting $A_xP_8W_8O_{40}$ one-dimensional bronzes.

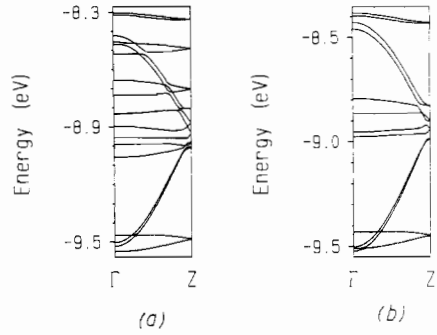


**Figure 7.** Dispersion relations of the $t_{2g}$-block bonds of (a) the $W_6O_{28}$ chain and (b) the $W_4O_{18}$ chain, where $\Gamma = 0$ and $Z = c^*/2$.

**Band Electronic Structure.** Figure 7a shows the dispersion relations of the $t_{2g}$-block bands calculated for the $W_6O_{28}$ chain (**2**). With four electrons to fill these bands, the Fermi level lies near the top of the bottom flat band, and the bottom dispersive bands become partially filled as well. The partially filled bands are largely represented by the tungsten atoms $W_I$ and $W_{II}$. This can be seen from Figure 7b, which shows the dispersion relations of the $t_{2g}$-block bands calculated for the $W_4O_{18}$ chain (**3**), obtained from the $W_6O_{28}$ chain by removing $W_{III}O_6$ octahedra. Clearly, the bottom portions of parts a and b of Figure 7 are nearly identical in nature. Consequently, the d electrons reside mainly in the $W_IO_6$ and $W_{II}O_6$ octahedra in agreement with the Zachariasen analysis. The orbital characters of the $t_{2g}$-block bands of the $W_4O_{18}$ chain are quite similar to those of the $Mo_4O_{18}$ chain, described in detail elsewhere[15] in connection with $Li_{0.9}Mo_6O_{17}$: The bottom flat band is of $\pi$ type (i.e., $xz$ and $yz$ orbitals), and the bottom dispersive band is of $\delta$ type (i.e., $x^2 - y^2$ orbitals).

From the band dispersions of the $W_6O_{28}$ and $W_4O_{18}$ chains, one might speculate a one-dimensional (1D) character for $P_8W_{12}O_{52}$. However, this is not the case as can be seen from Figure 8, which shows dispersion relations of the bottom portion of the $t_{2g}$-block bands calculated for the $W_{12}O_{48}$ lattice of $P_8W_{12}O_{52}$. The essential features of the band dispersions of the $W_{12}O_{48}$ lattice are similar to those of the $W_6O_{28}$ chain, except for an important difference that the $\pi$-type bands of the $W_{12}O_{48}$ lattice exhibit

(12) Wang, E.; Greenblatt, M. *J. Solid State Chem.* **1988**, *76*, 340.
(13) Benmoussa, A.; Groult, D.; Labbe, Ph.; Raveau, B. *Acta Crystallogr.* **1984**, *C40*, 573.
(14) Lamire, M.; Labbe, Ph.; Goreaud, M.; Raveau, B. *Rev. Chim. Miner.* **1987**, *24*, 153.
(15) Whangbo, M.-H.; Canadell, E. *J. Am. Chem. Soc.* **1988**, *110*, 358.

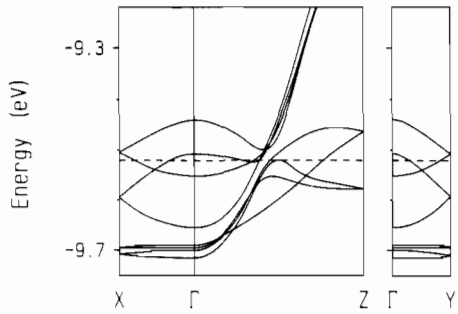


**Figure 8.** Dispersion relations of the bottom portion of the $t_{2g}$-block bands calculated for the $W_{12}O_{48}$ lattice of $P_8W_{12}O_{52}$, where the dashed lines refers to the Fermi level, $\Gamma = (0, 0, 0)$, $X = (a^*/2, 0, 0)$, $Y = (0, b^*/2, 0)$, and $Z = (0, 0, c^*/2)$.

substantial dispersions in all three directions. Since the $W_{12}O_{48}$ lattice has two $W_6O_{28}$ chains per unit cell, there are eight d electrons to fill the bands of Figure 8. Consequently, the $\pi$-type bands are cut by the Fermi level in all three directions, and $P_8W_{12}O_{52}$ is a 3D metal. It is of interest to examine why the $\pi$-type bands show dispersion in all three directions. As shown in Figure 1 and diagram **2**, the $W_{III}O_6$ octahedra of one $W_6O_{28}$ chain are linked to the $W_{II}O_6$ octahedra of the neighboring $W_6O_{28}$ chain. Therefore, the $\pi$-type orbitals of an $W_{III}O_6$ octahedron provide $\pi$-type interactions not only within a $W_6O_{28}$ chain but also between $W_6O_{28}$ chains, as schematically depicted in **4**. This

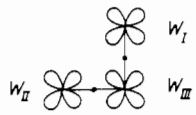


**4**

interchain interaction is effective in the low-lying $\pi$-type bands of $P_8W_{12}O_{52}$. A $W_{III}O_6$ octahedron of one $W_6O_{28}$ chain is linked in a tilted manner (due to the diphosphate ions) to a $W_{II}O_6$ octahedron of the neighboring $W_6O_{28}$ chain, which leads to a better interaction between the $W_{II}O_6$ and $W_{III}O_6$ octahedra. In addition, the $\pi$-type d-block levels of each $W_{III}O_6$ octahedron are somewhat lowered in energy by sharing their two oxygen atoms with the $W_{II}O_6$ octahedron of the neighboring $W_6O_{28}$ chain. This also leads to a greater participation of the $W_{III}O_6$ character in the low-lying $\pi$-type bands of the $W_{12}O_{48}$ lattice. The pseudo-1D bronze $CsP_8W_8O_{40}$ was found to lose its metallic character when more than 3% of W was replaced by Mo.[9] In contrast, $P_8W_{12}O_{52}$ remains a 3D metal even when 5% of W is replaced by Mo. This is understandable since the $W_{12}O_{48}$ lattice has a 3D connectivity of $WO_6$ octahedra via the $W_{III}O_6$ octahedra.

According to Figure 8, $P_8W_{12}O_{52}$ will behave like a 1D metal if more electrons are added to its lattice so that the Fermi level lies above the top of the $\pi$ bands. Our calculations show that this change requires more than four electrons per formula unit $P_8W_{12}O_{52}$. This explains why all the $A_xP_8W_{12}O_{52}$ (A = Li, Na; $x < 1$) bronzes are 3D metals. One might consider the possibility of preparing $Li_xP_8W_{12}O_{52}$ ($x > 4$) to see if it becomes a 1D metal, provided that the pentagonal and hexagonal channels of $P_8W_{12}O_{52}$ can accommodate enough Li atoms.

## Concluding Remarks

In summary, we prepared $P_8W_{12}O_{52}$ and its substituted analogues and measured their physical properties. All those bronzes are 3D metals and hence show no resistivity anomalies. Our tight-binding band electronic structure calculations show that this 3D metallic character arises from two factors: (a) The lattice of the $P_8W_{12}O_{52}$ has a 3D connection of $WO_6$ octahedra, and (b) $P_8W_{12}O_{52}$ has a small number of d electrons so that its 3D bands, occurring near the bottom of the $t_{2g}$-block bands, become partially filled. Our calculations predict that $A_xP_8W_{12}O_{52}$ (A = alkali metal) would remain a 3D metal unless $x > 4$. Finally, the close relationship between $P_8W_{12}O_{52}$ and $CsP_8W_8O_{40}$ structures was demonstrated by the intergrowth of these two bronzes and the phase transition from $P_8W_{12}O_{52}$ to $CsP_8W_8O_{40}$. Investigation of the phase transition led to a new synthetic route for the preparation of single crystals of Rb and Tl analogues of $CsP_8W_8O_{40}$.

**Acknowledgment.** Work at Rutgers University was supported in part by the Office of Naval Research, the National Science Foundation-Solid State Chemistry Grants DMR-84-04003 and DMR-87-14072, and the National Science Foundation Materials Research Instrumentation Grants DMR-84-08266 and DMR-87-05620. Work at the Universite de Paris-Sud and North Carolina State University was supported by NATO, Scientific Affairs Division, and also by DOE, Office of Basic Sciences, Division of Materials Science, under Grant DE-FG05-86ER45259.

---

Contribution from the Department of Applied Chemistry, Faculty of Engineering, Osaka University, Suita, Osaka 565, Japan

# Efficient Reduction of Dioxygen with Ferrocene Derivatives, Catalyzed by Metalloporphyrins in the Presence of Perchloric Acid

Shunichi Fukuzumi,*[1a] Seiji Mochizuki, and Toshio Tanaka[1b]

*Received November 28, 1988*

Reduction of dioxygen with ferrocene derivatives (Fc) is catalyzed by metalloporphyrins ($MTPP^+$: M = Co, Fe, Mn; TPP = tetraphenylporphyrin) or $Co(TIM)^{3+}$ (TIM: a tetraaza macrocyclic ligand) in the presence of $HClO_4$ in acetonitrile (MeCN). Electron transfer from Fc to $MTPP^+$ is the rate-determining step for the $MTPP^+$-catalyzed oxidation of Fc by dioxygen, when the rate is independent of the concentration of dioxygen or $HClO_4$. On the other hand, the rate of electron transfer from Fc to $Co(TIM)^{3+}$ is accelerated by the presence of $HClO_4$ and dioxygen. The rates of these electron-transfer reactions are discussed in light of the Marcus theory of electron transfer to distinguish between outer-sphere and inner-sphere electron-transfer processes. The strong inner-sphere nature of metalloporphyrins in the electron-transfer reactions with dioxygen in the presence of $HClO_4$ plays an essential role in the catalytic reduction of dioxygen.

Metalloporphyrin-catalyzed reduction of dioxygen has been extensively studied in the electrochemical system in conjunction with the search for an inexpensive cathode material for a dioxygen fuel cell,[2,3] and four-electron reduction of dioxygen to water has

0020-1669/89/1328-2459$01.50/0 